Improving the false alarm capabilities of the maximum average correlation height correlation filter

Mohamed Alkanhal, MEMBER SPIE
B. V. K. Vijaya Kumar, FELLOW SPIE
Carnegie Mellon University
Department of Electrical and Computer Engineering
Pittsburgh, Pennsylvania 15213

Abhijit Mahalanobis, FELLOW SPIE
Raytheon Missile Systems Company
Tucson, Arizona 85734

Abstract. We show that the maximum average correlation height (MACH) correlation filter overemphasizes the importance of the average training image leading to poor discrimination of the desired class images from clutter images. To overcome this, two new metrics termed the all image correlation height (AICH) and the modified average similarity measure (MASM) are introduced and optimized in a new correlation design. The resulting filter exhibits improved clutter rejection performance while retaining the attractive distortion tolerance feature of the MACH filter. Simulation results based on a simulated synthetic aperture radar (SAR) image database are presented to illustrate the new filter's properties.
[S0091-3286(00)01805-5]

Subject terms: maximum average correlation height filter; correlation; clutter; false alarm; synthetic discriminant function.

Paper ATR-021 received Sep. 24, 1999; revised manuscript received Nov. 22, 1999; accepted for publication Dec. 9, 1999.

1 Introduction

Correlation filters are attractive for automatic target recognition (ATR) because of their shift invariance and potential for distortion-tolerant pattern recognition. Despite much prior work,[1–6] one of the problems that still exists today in using correlation filters for ATR is the high false alarm rate when detecting targets in scenes containing noise and clutter. In this paper, we propose a new correlation filter design aimed at reducing the false alarms due to clutter.

In recent research,[7–9] correlation filters were shown to have excellent ATR performance. However, correlation filter response to nontraining images, in general, and clutter images, in particular, is not well understood. For example, correlation filters are usually designed using a training set of images from a desired class. The training set is selected to contain all expected variations of desired targets, but it rarely contains examples of the clutter. This is due to the difficulty of having a comprehensive clutter database or even knowing *a priori* what type of clutter images to expect. Essentially, every nontarget object of any size in a scene is a valid clutter example. Thus, sometimes, clutter images might be falsely detected as targets by correlation filters. We will generically refer to this false detection of clutter as a false alarm or a clutter rejection problem.

The original synthetic discriminant function (SDF) filter[10] is designed such that the correlation outputs of all training images take on specified values (e.g., same values for all training images in one class) at the origin. In vector notation, this is given by

$$\mathbf{X}^{+}\mathbf{h}=\mathbf{c}, \tag{1}$$

where $\mathbf{X}$ is a $d^2\times N$ matrix containing as column vectors lexicographically ordered versions of the 2-D Fourier transforms of the N training images (each with $d\times d=d^2$ pixels), $\mathbf{h}$ is a column vector with d^2 elements representing the correlation filter in the frequency domain, $\mathbf{c}$ is a column vector containing the correlation output constraints, and the superscript $^{+}$ represents the complex conjugate transpose. Matrices and vectors are denoted by bold uppercase and lowercase letters, respectively.

From Eq. (1), the original SDF filter can be seen to control only the origin value of the correlation output. Thus, the sidelobes are often higher than the target response at the origin, which makes the target location incorrect. The large sidelobe problem led Mahalanobis et al.[11] to propose the minimum average correlation energy (MACE) filter, one of the most popular SDF filters. The MACE filter is designed to minimize the average correlation energy (ACE) in the correlation output while satisfying the constraints in Eq. (1). The MACE filter improves discrimination and produces easily discernible peaks. In its attempt to produce sharp correlation peaks, however, the MACE filter emphasizes high frequencies and can result in poor intraclass recognition of images not included in the training set.

Fisher and Principe[12] introduced a nonlinear extension to the MACE filter. First, the input image to the nonlinear MACE filter is preprocessed by the same whitening operation used in the linear MACE filter. The output is input to an artificial neural network. Although their results exhibited good clutter rejection performance, this method can be computationally expensive due to the nonlinear neural network structure.

The SDF filters discussed in the preceding and many other variants attempt to satisfy Eq. (1). These constraint values are loosely referred to as the correlation peaks, although there is no guarantee that the peak is always at the origin. It was observed[13] that placing such constraints un-

necessarily restricts the filters. It means even less in the presence of distortions since the correlation peaks for test images from the desired class will differ anyway from those of the training images. By removing or relaxing the constraints in Eq. (1), the number of possible solutions is increased, providing a better chance for finding a solution with better performance. Recently, some new correlation filter designs based on soft constraints were proposed.[13–17] The maximum average correlation height (MACH) filter[13] is an important example of such unconstrained filters.

The MACH filter relaxes the correlation peak constraints and maximizes the peak intensity of the average training image. The peak intensity of the average training image is $|\bar{g}(0,0)|^2$, where

$$|\bar{g}(0,0)|^2=\left|\frac{1}{N}\sum_{i=1}^{N}\mathbf{h}^{+}\mathbf{x}_i\right|^2=|\mathbf{h}^{+}\mathbf{m}|^2, \tag{2}$$

where $\mathbf{m}=(1/N)\Sigma_{i=1}^{N}\mathbf{x}_i$ is the Fourier transform of the average of the N training images. The MACH filter also optimizes the distortion tolerance by minimizing a metric that characterizes the dissimilarity in the correlation output shape between all training images and their average. This metric known as the average similarity measure (ASM) can be written as

$$\mathrm{ASM}=\mathbf{h}^{+}\mathbf{S}_x\mathbf{h}, \tag{3}$$

where

$$\mathbf{S}_x=\frac{1}{N}\sum_{i=1}^{N}(\mathbf{X}_i-\mathbf{M})^{+}(\mathbf{X}_i-\mathbf{M}), \tag{4}$$

where $\mathbf{X}_i$ is a diagonal matrix containing vector $\mathbf{x}_i$ along its main diagonal, and $\mathbf{M}$ is a diagonal matrix containing $\mathbf{m}$ along its diagonal. Thus $\mathbf{S}_x$ is a $d^2\times d^2$ diagonal matrix.

Initial results showed that the MACH filter could reduce the number of missed targets and provide better generalization compared to the MACE filter.[13] In addition, the computation of the MACH filter is easier compared to the MACE filter since it does not require any matrix inversion. While the average training image used in the MACH filter design is good in representing the average behavior of the desired class, it fails to capture the finer details of the desired class. In fact, the average of training images sometimes looks like a clutter image. Thus, the MACH filter may prove inadequate in discriminating the desired class from the clutter causing increased false alarm rate. In this paper, we introduce the extended MACH (EMACH) filter aimed at improving the clutter rejection capability.

The rest of this paper is organized as follows. Section 2 reviews the MACH filter design to help clarify the causes of its false alarm. Section 3 introduces the EMACH filter designed to improve sensitivity against clutter. In Sec. 4, we discuss the synthetic aperture radar (SAR) ATR system and the database we used to test the MACH and EMACH filters. In Sec. 5, we demonstrate the improved ability of the EMACH filter to recognize SAR targets in real clutter while achieving a low false alarm rate compared to the MACH filter.

2 MACH Filter and the False Alarm Problem

It has been shown[6] that the MACH filter exhibits better distortion tolerance performance than other linear SDF filters. This is due to the inclusion of the ASM criterion, which increases the filter's distortion tolerance and also perhaps due to its unconstrained design. We briefly review the synthesis of the MACH filter to clarify its clutter rejection problem.

The MACH filter is designed to maximize the intensity of the average correlation output at the origin due to training images. The average of correlation peaks is the correlation output due to the average training image. It also maximizes the similarity between the average training image correlation output and those outputs due to all training images from the desired class. Hence, in a sense, the MACH filter forces all images from the desired class to follow the behavior of the average training image from that class.

Also, to maintain some degree of noise tolerance in the MACH filter design, output noise variance (ONV) is also included in the optimization. It can be shown that ONV $=\mathbf{h}^{+}\mathbf{h}$ for additive white noise (where we assumed that the white noise two-sided power spectral density variance is 1 without any loss of generality). Hence, the MACH filter criterion can be written as

$$J(\mathbf{h})=\frac{|\bar{g}(0,0)|^2}{\mathbf{h}^{+}\mathbf{h}+\mathbf{h}^{+}\mathbf{S}_x\mathbf{h}}, \tag{5}$$

where $|\bar{g}(0,0)|^2$ and $\mathbf{S}_x$ are defined in Eqs. (2) and (4), respectively.

In Eq. (5), $\mathbf{h}^{+}\mathbf{S}_x\mathbf{h}$ represents the ASM metric, which quantifies the similarity (actually the dissimilarity) of the correlation output plane due to individual training images from their average. Although we simply added ONV and ASM in Eq. (5), we can weight them differently before the addition. Maximizing $J(\mathbf{h})$ with respect to $\mathbf{h}$ leads to the following[13]:

$$\mathbf{h}=(\mathbf{I}+\mathbf{S}_x)^{-1}\mathbf{m}. \tag{6}$$

Thus the MACH filter relies heavily (perhaps too heavily) on the mean training image. It amplifies the high-energy (usually low-frequency) components of the training set and at the same time attenuates the low-energy (usually high-frequency) components of the training set. Thus, by using this $\mathbf{m}$ as the only example that represents all training images, we may get a filter that does not capture the finer details of the training images. This might lead the filter to not discriminate the desired class from the clutter.

To illustrate the clutter rejection problem, Fig. 1 shows a 41×41-pixel image of digit 3, from which we obtained 180 rotated images by rotating this image in plane by 2-deg increments. Figure 2 shows the digit 3 at different rotation angles. The average of all 180 images is shown in Fig. 3. The average looks like a ''blob'' more than an image from the desired class. This suggests that the average training image is not necessarily a good representative of the desired class. Of course, the average might look more like a training image if we had used a much smaller range of distortions.

Fig. 1 A 41- $\times$41-pixel image of digit 3.

The MACH filter maximizes the correlation peak due to the average training image. Let us assume that

$$\mathbf{h}^{+}\mathbf{x}_i = \text{peak}_i \quad i = 1,2,\ldots,N. \tag{7}$$

Ideally, we want all clutter images to result in correlation outputs smaller than $\text{peak}_{\min}$, where $\text{peak}_{\min}$ is the smallest among $\{\text{peak}_1, \text{peak}_2, \ldots, \text{peak}_N\}$, i.e., the peaks for the training images. However, let us consider the correlation output due to images in the convex hull ψ of the training set. The convex hull ψ can be defined as the smallest convex set containing all training images, i.e.,

$$\psi = \left\{ \mathbf{x}: \mathbf{x} = \sum_{i=1}^{N} \lambda_i \mathbf{x}_i, \lambda_i \geqslant 0, \sum_{i=1}^{N} \lambda_i = 1 \right\}. \tag{8}$$

Some of the images in the convex hull are more like clutter than like the desired class (see Fig. 3, showing the average, which is one such point in the convex hull corresponding to $\lambda_i = 1/N$ for $i = 1,2,\ldots,N$). For any image $\mathbf{x}$ in the convex hull, the MACH filter output will be larger than or equal to $\text{peak}_{\min}$ as shown in the following.

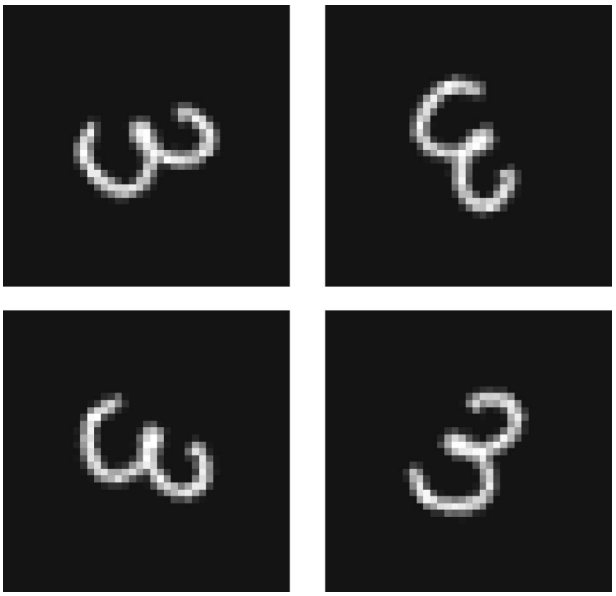

Fig. 2 Four images of different in-plane-rotated versions of the digit 3 image of Fig. 1.

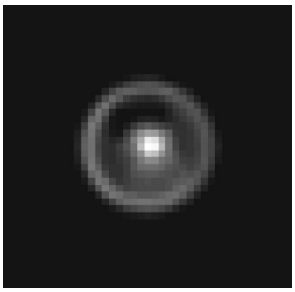

Fig. 3 Average of the 180 in-plane-rotated versions of digit 3, it does not look like 3.

$$\mathbf{h}^{+}\mathbf{x} = \sum_{i=1}^{N} (\lambda_i \mathbf{h}^{+}\mathbf{x}_i)$$

$$\geqslant \sum_{i=1}^{N} (\lambda_i \text{peak}_{\min}) = \text{peak}_{\min} \sum_{i=1}^{N} \lambda_i = \text{peak}_{\min}. \tag{9}$$

Equation (9) means that the MACH filter will yield larger peaks for some clutter images in the convex hull than for the training images. Figure 4(a) shows the MACH filter (designed using 180 training images of the digit 3) correlation output for one of the training images, and Fig. 4(b) shows the output for the average training image shown in Fig. 3. The correlation output for the average image is similar to, if not better than, that due to the training images, although the average image looks more like clutter than the digit 3.

From this simple demonstration, we conclude that the MACH filters (and in fact many SDF filters) possess attributes that make them falsely detect clutter images as targets. One such attribute is that all training images follow the same behavior as the average training image. However, the average training image is not necessarily a good representative of the desired class. Another way to state this is that we must take great pains to make sure that the average image is not very different from the training images.

3 EMACH

As stated in Sec. 2, the MACH filter probably overemphasizes the importance of the average training image and thus might fail in discriminating the desired class from clutter. Hence, we must control the relative contribution of the desired class training images as well as their average. Toward that goal, we introduce a new metric called all image correlation height (AICH):

$$\text{AICH} = \frac{1}{N} \sum_{i=1}^{N} (\mathbf{h}^{+}\mathbf{x}_i)^2 - \alpha (\mathbf{h}^{+}\mathbf{m})^2, \tag{10}$$

where α is a parameter that takes on a value between 0 and 1 and governs the relative significance of the average training image in the filter design. It is easy to show that AICH in Eq. (10) can also be written as

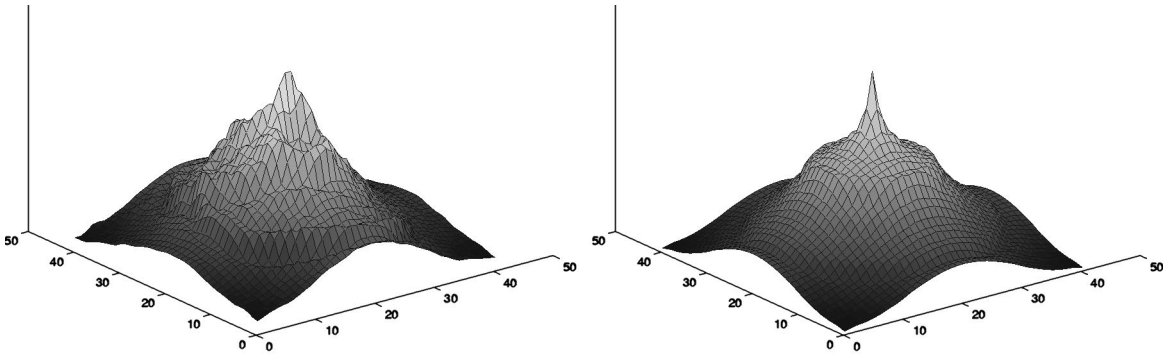

Fig. 4 MACH filter correlation output (a) for training image at 0 deg and (b) for the average training image shown in Fig. 3.

$$\text{AICH}=\frac{1}{N}\sum_{i=1}^{N}[\mathbf{h}^{+}(\mathbf{x}_i-\beta\mathbf{m})]^2$$
$$=\frac{1}{N}\sum_{i=1}^{N}(\mathbf{h}^{+}\mathbf{x}_i-\beta\mathbf{h}^{+}\mathbf{m})^2$$
$$=\frac{1}{N}\sum_{i=1}^{N}(\mathbf{h}^{+}\mathbf{x}_i)^2-(2\beta-\beta^2)(\mathbf{h}^{+}\mathbf{m})^2, \quad (11)$$

provided $\alpha=2\beta-\beta^2$. Equivalently, α and β are related by $\beta=1\pm\sqrt{1-\alpha}$. Thus as α varies between 0 and 1, β varies between 0 and 2. From here on, we refer only to β and ignore α. By controlling β, the designed filter is prevented from being overwhelmed by the biased treatment of the low-frequency components represented by the average image. Here, we must optimize the AICH. To be able to do that, we rewrite Eq. (11) as

$$\text{AICH}=\frac{1}{N}\sum_{i=1}^{N}(\mathbf{h}^{+}\mathbf{x}_i-\beta\mathbf{h}^{+}\mathbf{m})^2$$
$$=\frac{1}{N}\sum_{i=1}^{N}(\mathbf{h}^{+}\mathbf{x}_i-\beta\mathbf{h}^{+}\mathbf{m})(\mathbf{h}^{+}\mathbf{x}_i-\beta\mathbf{h}^{+}\mathbf{m})^{+}$$
$$=\mathbf{h}^{+}\left[\frac{1}{N}\sum_{i=1}^{N}(\mathbf{x}_i-\beta\mathbf{m})(\mathbf{x}_i-\beta\mathbf{m})^{+}\right]\mathbf{h}=\mathbf{h}^{+}\mathbf{C}_x^{\beta}\mathbf{h}, \quad (12)$$

where

$$\mathbf{C}_x^{\beta}=\frac{1}{N}\sum_{i=1}^{N}(\mathbf{x}_i-\beta\mathbf{m})(\mathbf{x}_i-\beta\mathbf{m})^{+}. \quad (13)$$

Thus, as shown in Eq. (11), AICH can be described as the average of the correlation peak intensities of N exemplars where the ith exemplar $(\mathbf{x}_i-\beta\mathbf{m})$ is the i'th training image with part of the mean subtracted. Hence, it is desirable for all images in the training set to follow these exemplars' behavior. This can be done by forcing every image in the training set $\mathbf{x}_i$ to have a similar correlation output plane to an ideal correlation output shape $\mathbf{f}$. To find the $\mathbf{f}$ that best matches all these exemplars' correlation output planes, we minimize its deviation from their correlation planes. This deviation can be quantified by the average squared error (ASE):

$$\text{ASE}=\frac{1}{N}\sum_{i=1}^{N}(\mathbf{g}_i-\mathbf{f})^{+}(\mathbf{g}_i-\mathbf{f}), \quad (14)$$

where

$$\mathrm{g}=(\mathbf{X}_i-\beta\mathbf{M})\mathbf{h}^{*}, \quad (15)$$

where the superscript * represents the complex conjugate.

To find the optimum shape vector $\mathbf{f}_{\text{opt}}$, we set the gradient of ASE with respect to $\mathbf{f}$ to zero. Then, we obtain

$$\mathbf{f}_{\text{opt}}=\frac{1}{N}\sum_{i=1}^{N}\mathbf{g}_i=\frac{1}{N}\sum_{i=1}^{N}(\mathbf{X}_i-\beta\mathbf{M})\mathbf{h}^{*}=(1-\beta)\mathbf{M}\mathbf{h}^{*}. \quad (16)$$

Now, we modify the ASM such that it measures the dissimilarity of the training images to $(1-\beta)\mathbf{M}\mathbf{h}^{*}$. We call this new measure the modified ASM (MASM).

$$\text{MASM}=\frac{1}{N}\sum_{i=1}^{N}[\mathbf{X}_i\mathbf{h}^{*}-(1-\beta)\mathbf{M}\mathbf{h}^{*}]^{+}$$
$$\times[\mathbf{X}_i\mathbf{h}^{*}-(1-\beta)\mathbf{M}\mathbf{h}^{*}]$$
$$=\mathbf{h}^{T}\left\{\frac{1}{N}\sum_{i=1}^{N}[\mathbf{X}_i-(1-\beta)\mathbf{M}]^{*}[\mathbf{X}_i-(1-\beta)\mathbf{M}]\right\}\mathbf{h}^{*}$$
$$=\mathbf{h}^{T}\mathbf{S}_x^{\beta}\mathbf{h}^{*}=\mathbf{h}^{+}\mathbf{S}_x^{\beta}\mathbf{h}, \quad (17)$$

where the superscript T represents the transpose and where we used the fact that MASM is real in deriving the last equality in Eq. (17). The diagonal matrix $\mathbf{S}_x^{\beta}$ is given by

$$\mathbf{S}_x^{\beta}=\frac{1}{N}\sum_{i=1}^{N}[\mathbf{X}_i-(1-\beta)\mathbf{M}]^{*}[\mathbf{X}_i-(1-\beta)\mathbf{M}]. \quad (18)$$

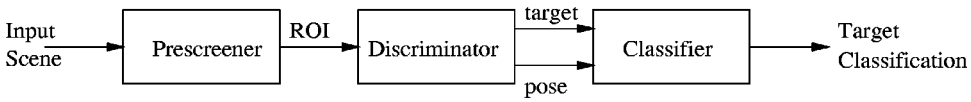

Fig. 5 Block diagram of ATR SAR system.

As we know, the ASM is a good measure for distortion tolerance; however, it lacks some discrimination capability that explains part of the MACH filter's inability to reject some clutter images. On the other hand, the MASM measure captures finer details of training set that makes the new designed filter more sensitive against clutter. This can be more easily seen when Eq. (17) is rewritten as

$$\text{MASM}=\mathbf{h}^{+}\left(\frac{1}{N}\sum_{i=1}^{N}\mathbf{X}_i^{*}\mathbf{X}_i\right)\mathbf{h}-(1-\beta^2)\mathbf{h}^{+}\mathbf{M}^{*}\mathbf{M}\mathbf{h}$$
$$=\mathbf{h}^{+}\mathbf{D}_x\mathbf{h}-(1-\beta^2)\mathbf{h}^{+}\mathbf{M}^{*}\mathbf{M}\mathbf{h}. \quad (19)$$

As we increase β, the MASM measure emphasizes the ACE term $\mathbf{h}^{+}\mathbf{D}_x\mathbf{h}$ and thus the influence of high-frequency components is maximized compared to the ASM measure.

By maximizing the AICH (i.e., balancing the significance of the training images frequency components) and minimizing the MASM while controlling the parameter β, we hope to explicitly keep a balance between the distortion tolerance and clutter rejection performance. Therefore, we propose to optimize the following new criterion:

$$J^{\beta}(\mathbf{h})=\frac{\text{AICH}}{\mathbf{h}^{+}\mathbf{h}+\mathbf{h}^{+}\mathbf{S}_x^{\beta}\mathbf{h}}=\frac{\mathbf{h}^{+}\mathbf{C}_x^{\beta}\mathbf{h}}{\mathbf{h}^{+}(\mathbf{I}+\mathbf{S}_x^{\beta})\mathbf{h}}, \quad (20)$$

where $\mathbf{h}^{+}\mathbf{h}$ is the ONV term assuming an additive white noise with unit variance. ONV helps maintain noise tolerance when β increases especially at those low energy components.

By maximizing the preceding criterion, we get the following condition for the EMACH filter

$$(\mathbf{I}+\mathbf{S}_x^{\beta})^{-1}\mathbf{C}_x^{\beta}\mathbf{h}=\lambda\mathbf{h}, \quad (21)$$

where λ is a scalar identical to $J^{\beta}(\mathbf{h})$.

Thus, $\mathbf{h}$ must be an eigenvector of $(\mathbf{I}+\mathbf{S}_x^{\beta})^{-1}\mathbf{C}_x^{\beta}$ with the corresponding eigenvalue λ. Since λ is identical to $J(\mathbf{h})$, $\mathbf{h}$ should be the eigenvector that corresponds to the maximum eigenvalue. The other eigenvectors corresponding to the other nonzero eigenvalues provide smaller $J^{\beta}(\mathbf{h})$ values. However, they may provide better discriminatory performance, as β is not known beforehand. A computational method for determining these eigenvectors and their corresponding eigenvalues [of Eq. (21)] can be found in Ref. 18.

4 SAR ATR Architecture

We investigate the advantages of the EMACH filter in the ATR of SAR imagery. SAR sensors provide high resolution, range invariance (within limits), and all-weather capability. However, there are some obvious difficulties for recognizing targets in SAR imagery. These include target variability with aspect and depression angle, and speckle noise present in SAR images.[19] Correlation filters were first applied for SAR ATR by Mahalanobis et al.[20] with significant success. The early SDF filters for SAR ATR have been improved significantly with the use of MACH/distance classifier correlation filter (DCCF) approaches.[8,9]

Our SAR ATR architecture is shown in Fig. 5. The system is composed of three stages. In the first stage, the prescreener processes a wide-area single SAR scene that may contain multiple targets. The outputs of the prescreener are sections of size 64×64 pixels called regions of interest (ROIs) that are flagged as containing potential targets. These ROI images, which form a small part of the original scene, are processed by the discriminator in the second stage. The goal of the discriminator is to reject natural-clutter objects (e.g., trees, terrain) while passing man-made objects, which include targets as well as man-made clutter (e.g., cars, bridges, roads). To increase the processing speed, the discriminator estimates the pose (aspect angle) of the object. Since the pose estimate is based on the length to width ratio, the angle estimate usually has an ambiguity of 180 deg. At the end, a correlation filter in the classification stage will take as its input each of the SAR ROI images passed by the discriminator along with their pose estimates and produces a correlation output. These SAR ROIs will be assigned to either the desired class or clutter based on the peak-to-sidelobe ratio (discussed in Sec. 4.2) of their correlation outputs.

4.1 *Database*

We used the simulated SAR images to build and test the MACH and EMACH filters. Simulated SAR imagery were generated with the radar prediction program known as Xpatch.[21] A model of a T72 tank was used at various aspects all at a 40-deg depression angle. The data set contains 360 images, one for each rotation aspect angle increment of 1 deg, each of size 64×64 pixels of 8 -bit resolution with a zero background. These images were scaled to match the dynamic range of a set of real SAR images.

In this paper, 64 images at angular increments of 6 deg (i.e., 1, 7, 13 deg, . . .) were used for training. These training images have their zero background replaced by a constant value of 100 so that the designed filter does not get tuned to the high-frequency edges associated with training images in zero background.[22] Figure 6 shows some examples of these training images. Sixty-four target images from the same range that differ by 3 deg from the training images (i.e., 4, 10, 16 deg, . . .) were each inserted into five different real SAR backgrounds. These resulting 320 images were used as test images. As we can see in Fig. 7, target objects are slightly brighter than background which makes the ATR problem more difficult. Also, 540 clutter images were used to test the correlation filters. These clutter images passed both the screener and the discrimination stages. Some examples of them are shown in Fig. 8. These clutter images are comprised mainly of man-made clutter objects. They

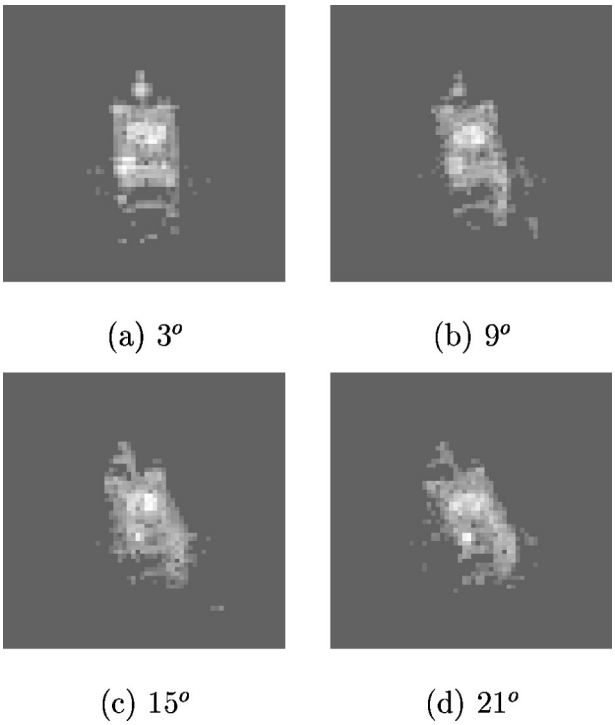

Fig. 6 Training images of size 64×64 of T72 tank shown at aspect angles 3, 9, 15 and 21 deg; the background value is 100.

also have a few natural clutter images, which passed the discrimination stage due to their bright returns.

4.2 *Performance Measures*

In this section, we discuss the two performance measures used to evaluate and compare the outputs of the MACH and EMACH filters.

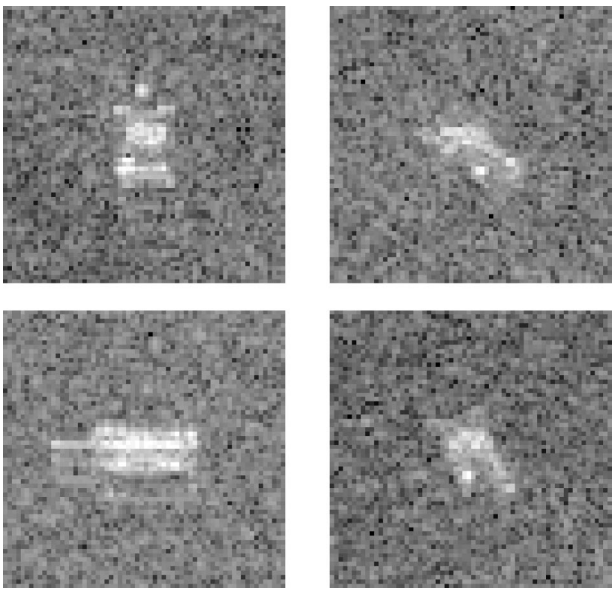

Fig. 7 Test images of size 64×64 of T72 tank shown at different aspect angles; the background is real clutter.

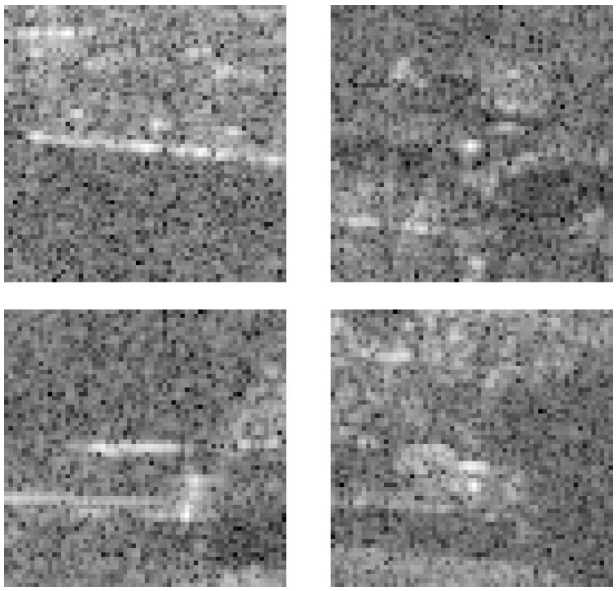

Fig. 8 Real SAR images of size 64×64 of man-made objects (i.e., cultural clutter).

4.2.1 *Peak-to-sidelobe ratio*

One of the primary concerns while detecting targets in input scene when using correlation filters is the detectability of the correlation peaks. This feature helps locate the target accurately. For such an ability, it is important for the correlation peaks to be sharp enough. A good measure for the peak sharpness is the peak-to-sidelobe ratio[23,24] (PSR):

$$\mathrm{PSR}=\frac{\text{peak}-\text{mean}}{\text{standard deviation}}=\frac{p-\mu}{\sigma}, \tag{22}$$

where p is the peak of the correlation output, and μ and σ are the mean and standard deviation, respectively, calculated over all pixels in the correlation output.

4.2.2 *Fisher ratio*

Discriminability, which refers to the filter's ability to discriminate between the desired class and the clutter, is an important attribute we want in correlation filters. A good measure of the discriminability is the Fisher ratio[25] (FR):

$$\mathrm{FR}=\frac{(m_1-m_2)^2}{\sigma_1^2+\sigma_2^2}, \tag{23}$$

where m_1 and σ_1^2 are the (sample) PSR mean and variance of the first class, and m_2 and σ_2^2 are the (sample) PSR mean and variance of the second class. Higher FR values indicate better separation between the two classes. Equation (23) shows that a large difference between the two means does not imply good performance unless we have relatively small variations within the PSR of each class.

5 Results

In this section, we discuss the performance results of the MACH and EMACH filters using the simulated SAR database described in Sec. 4.1. These filters were used in the

classification stage of the SAR ATR system described in Sec. 4. We synthesized a bank of MACH and EMACH filters with different β values for eight different aspect bins. Each one of these bins covers an aspect range of 45 deg. Since our training images are separated by 6 deg, every eight of them were used to build one filter. Because the classification stage is provided only with the pose estimate, two filters work (e.g., 0 and 180 deg, 45 and 225 deg. etc.) as a pair for our SAR ATR system. Thus, when we want to classify a SAR ROI image, a filter pair is first selected based on the pose estimate. Then, PSR measures are calculated at the outputs of the two filters and the maximum one is selected.

Figure 9 shows the correlation peaks of the EMACH and MACH filters for a test image at 352 (i.e., -8 deg) deg aspect angle. These outputs were generated by the filter pair spanning the pose estimate range from -24 to 22 deg. Figure 9(c) shows that the correlation peak of the EMACH filter with $\beta=0.45$ is sharper than that of the MACH filter shown in Fig. 9(b). This makes it easier to locate targets using the EMACH filter. This sharpness can be compared quantitatively using the PSR measure, which is 17.68 for the EMACH filter compared to 6.07 for the MACH filter. Also, the correlation output in Fig. 9(c) exhibits a desirable slight broadness, which indicates the distortion tolerance feature of the EMACH filter. The correlation output of the EMACH filter in Fig. 9(c) shows a smoother correlation output plane compared to that of the MACH filter. This indicates the EMACH filter's improved clutter rejection capability.

With the PSR features we calculated the FR between the desired and clutter images for all MACH and EMACH filter pairs for different β values. Table 1 shows the FR measures for all MACH and EMACH filter pairs. The β values shown are the best in terms of the FR. It is clear that the EMACH filter exhibits a significant improvement in terms of the FR over the MACH filter, which indicates a better separation between the PSR measures. Figure 10 shows the behavior of the FR measures of the EMACH filter when changing β for all four filter pairings. In general, Fig. 10 shows that the EMACH filter at $\beta=0$ exhibits a comparable performance to the MACH filter. It also indicates that the FR improves as β increases within a small range. Beyond that, the EMACH filter exhibits almost a stable performance for a long range of β. After this long range, the FR shows a degradation in the performance. This is due to the fact that β governs the contribution of the low-frequency components, which are represented by the average training image. As β increases beyond a certain value, the high-frequency components will be overemphasized over the low-frequency components, which leads to a filter sensitive to noise and distortions.

To show the trade-off between the probability of false alarm and the probability of detection, we calculated the receiver operating curves (ROCs) with the four filter pairs for the EMACH and MACH filters, as shown in Fig. 11. The β parameter used to synthesize the EMACH filter are the best in terms of the FR measure. The EMACH ROCs are not shown for the filter pairs spanning the pose estimates that range from 22 to 68 degrees and 68 to 112 degrees since we observed no false alarms for these two ranges. Fig. 11 shows that the EMACH filter performance

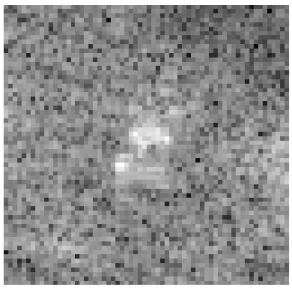

(a) test image at 352 degrees aspect angle

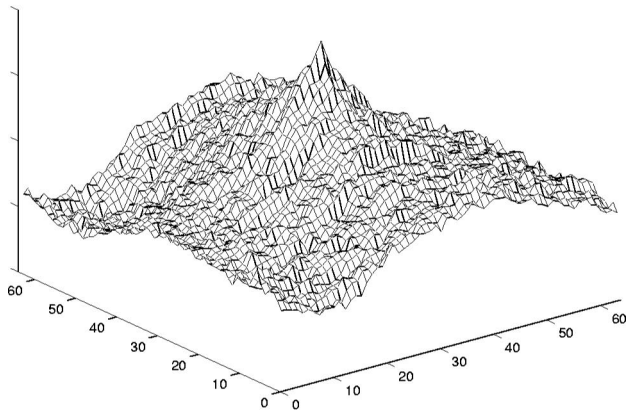

(b) MACH filter

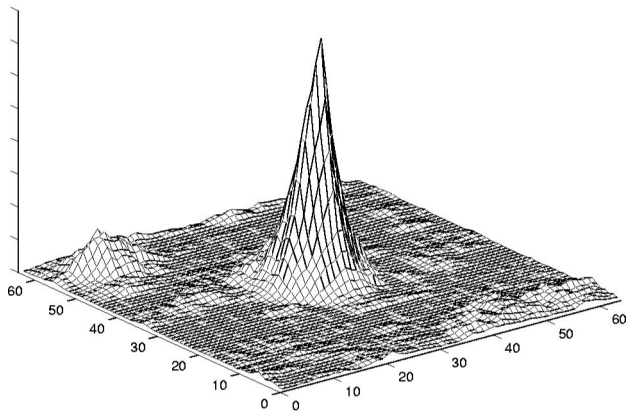

(c) EMACH filter ($\beta = 0.45$)

Fig. 9 (a) Test image and correlation outputs of the (b) MACH and the (c) EMACH filters for test image in (a).

is better than that of the MACH filter for all pose estimate ranges.

6 Conclusions

The original MACH filter has been shown to exhibit better distortion tolerance than other linear SDF filters. This was achieved by including the ASM and also by its unconstrained design. In spite of these attractive features, we have illustrated in this paper that the MACH filter overrelies on the average training image and thus might falsely

Table 1 FR measures for the MACH and EMACH filter pairs.

Filter Pair	MACH	EMACH
1	1.91	8.51 at $\beta=0.45$
2	2.81	12.83 at $\beta=0.30$
3	9.93	14.68 at $\beta=0.07$
4	2.94	9.97 at $\beta=0.40$

The β values are approximately those that give the best FR measures for the EMACH filter.

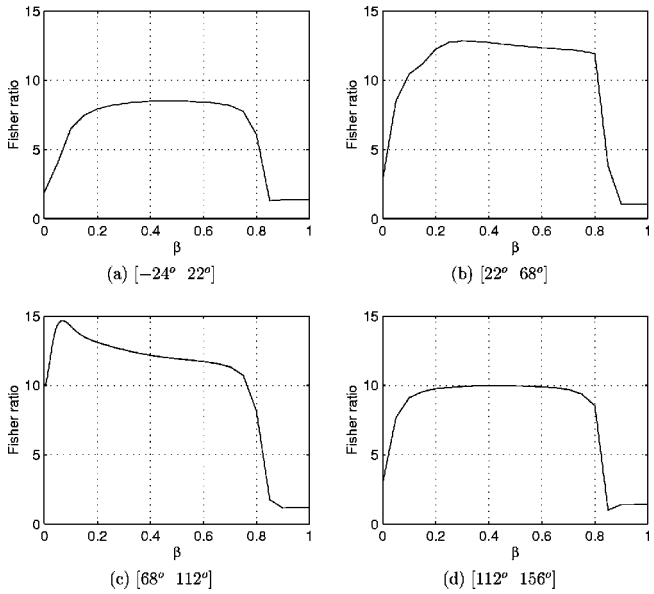

Fig. 10 FR as a function of β for all four different filter pairings. The ranges shown are for the pose estimates.

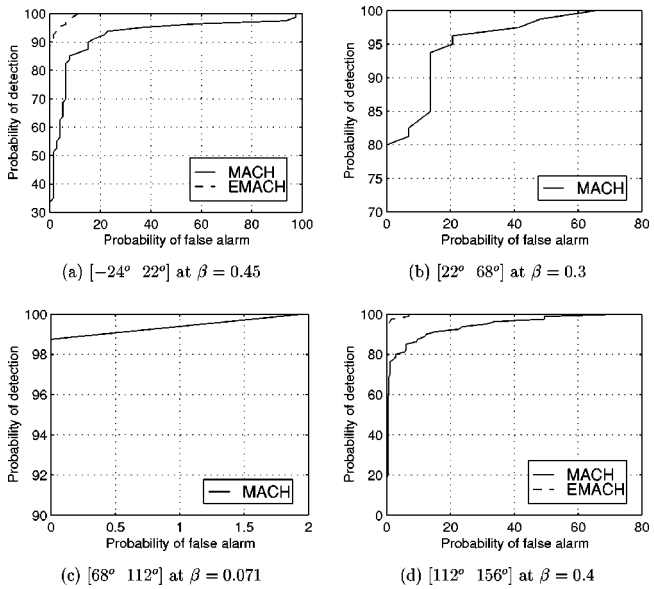

Fig. 11 ROCs for all four different filter pairings of the MACH (solid line) and EMACH (dashed line) filters at the best values of β.

detect clutter images as targets. To overcome this clutter rejection problem, we have modified the ACH to a new metric called the AICH, which enables us to weight the contribution of individual training images as well as their average. The AICH has led us to generalize the concept of the ASM to a new metric called the MASM. This MASM helps balance the treatment of discrimination and distortion tolerance in the filter design.

We used the new AICH and MASM measures to design a new correlation filter called the EMACH filter. In our tests, the EMACH filter showed better FRs and better recognition results compared to the MACH filter. This improvement is achieved by selecting the proper β parameter that makes the EMACH filter more sensitive to clutter images while retaining the distortion tolerance feature of the MACH filter.

References

1. H. J. Caulfield and W. T. Maloney, ''Improved discrimination in optical character recognition,'' *Appl. Opt.* **8**, 2354–2356 (1969).
2. R. R. Kallman, ''The construction of low noise optical correlation filters,'' *Appl. Opt.* **25**, 1032–1033 (1986).
3. P. Refregier, ''Filter design for optical pattern recognition: multicriteria optimization approach,'' *Opt. Lett.* **15**, 854–856 (1990).
4. D. L. Flannery and J. L. Horner, ''Fourier optical signal processors,'' *Proc. IEEE* **77**, 1511–1527 (1989).
5. B. V. K. Vijaya Kumar, ''Tutorial survey of composite filter designs for optical correlators,'' *Appl. Opt.* **31**, 4773–4801 (1992).
6. B. V. K. Vijaya Kumar and A. Mahalanobis, ''Recent advances in distortion-invariant correlation filter design,'' *Proc. SPIE* **2490**, 2–13 (1995).
7. D. W. Carlson, B. V. K. Vijaya Kumar, R. Mitchell, and M. Hoffelder, ''Composite correlation filters for SAR image recognition,'' *Proc. SPIE* **2757**, 338–349 (1996).
8. A. Mahalanobis, D. W. Carlson, and B. V. K. Vijaya Kumar, ''Evaluation of MACH and DCCF correlation filters for SAR ATR using MSTAR public data base,'' *Proc. SPIE* **3370**, 460–468 (1998).
9. A. Mahalanobis, L. Ortiz, and B. V. K. Vijaya Kumar, ''Performance of the MACH filter and DCCF algorithms on the 10-class public release MSTAR data set,'' *Proc. SPIE* **3721**, 285–291 (1999).
10. C. F. Hester and D. P. Casasent, ''Multivariant technique for multiclass pattern recognition,'' *Appl. Opt.* **19**(11), 1758–1761 (1980).
11. A. Mahalanobis, B. V. K. Vijaya Kumar, and D. Casasent, ''Minimum average correlation energy filters,'' *Appl. Opt.* **26**(17), 3633–3640 (1987).
12. J. Fisher III and J. Principe, ''Recent advances to nonlinear minimum average correlation energy filters,'' *Opt. Eng.* **36**(10), 2697–2709 (1997).
13. A. Mahalanobis, B. V. K. Vijaya Kumar, S. Song, S. R. F. Sims, and J. F. Epperson, ''Unconstrained correlation filters,'' *Appl. Opt.* **33**(17), 3751–3759 (1994).
14. A. Mahalanobis, B. V. K. Vijaya Kumar, and S. R. F. Sims, ''Distance classifier correlation filters for distortion tolerance, discrimination and clutter rejection,'' *Proc. SPIE* **2026**, 325–335 (1993).
15. D. W. Carlson, ''Optimal tradeoff composite correlation filters,'' PhD Thesis, Dept. of ECE, Carnegie Mellon University (Dec. 1996).
16. A. Mahalanobis and B. V. K. Vijaya Kumar, ''Polynomial filters for higher order and multi-input information fusion,'' in *Proc. 11th Euro American Opto-Electronic Information Processing Workshop*, pp. 221–231, Spain (June 1997).
17. R. Shenoy and D. Casasent, ''Correlation filters that generalize well,'' *Proc. SPIE* **3386**, 100–110 (1998).
18. A. Mahalanobis, B. V. K. Vijaya Kumar, and S. R. F. Sims, ''Distance-classifier correlation filters for multiclass target recognition,'' *Appl. Opt.* **35**(17), 3127–3133 (1996).
19. J. C. Curlander and R. N. McDonough, *Synthetic Aperture Radar: Systems and Signal Processing*, Wiley, New York (1991).
20. A. Mahalanobis, A. Forman, M. Bower, N. Day, and R. Cherry, ''A quadratic distance classifier for multi-class SAR ATR using correlation filters,'' *Proc. SPIE* **1875**, 84–95 (1993).
21. *User's Manual for Xpatch*, DEMACO Inc. (June 1995).
22. J. M. Florence, ''Design considerations for phase-only correlation filters,'' *Proc. SPIE* **69**, 195–202 (1990).
23. H. Mostafavi and F. Smith, ''Image correlation with geometric distortion, part II: effect of local accuracy,'' *IEEE Trans. Aerosp. Electron. Syst.* **14**, 496–501 (1978).
24. B. V. K. Vijaya Kumar and D. Casasent, ''Space-blur bandwidth product in correlator performance evaluation,'' *J. Opt. Soc. Am.* **70**, 103–110 (1980).

25. R. Duda and P. Hart, *Pattern Classification and Scene Analysis*, John Wiley, New York (1973).

Mohamed Alkanhal received his BS (honors) degree from King Saud University, Saudi Arabia, in 1993, and his MS degree in computer engineering from University of Southern California in 1995. He is currently working toward a PhD degree in electrical and computer engineering at Carnegie Mellon University. His interests are pattern recognition and multimedia communications. He is a student member of IEEE and SPIE.

B. V. K. Vijaya Kumar received his BTech and MTech degrees in electrical engineering from the Indian Institute of Technology (IIT), Kanpur, and his PhD in electrical engineering from Carnegie Mellon University (CMU), Pittsburgh. Since 1982, he has been a faculty member in the Department of Electrical and Computer Engineering at CMU, where he is now a professor. He also served as its associate department head from July 1994 through June 1996. Professor Kumar has done extensive research in several areas including pattern recognition, artificial neural networks, error control coding, and signal processing for data storage systems. He has authored or coauthored more than 230 technical papers in these areas. He served as a topical editor for the Information Processing Division of *Applied Optics*. Professor Kumar is a member of Sigma Xi, a senior member of IEEE and a fellow of SPIE and OSA. He is listed in Marquis' *Who's Who* in *Optical Sciences and Engineering* and in the *American Men and Women of Sciences*.

Abhijit Mahalanobis is a senior principle systems engineer in the Electro-Optics Department at Raytheon Missile Systems Company, Tucson, Arizona. His main interest are multisensor automatic target recognition, pattern recognition, and image processing with over 80 journal and conference publications in this area. He is currently the technical head for ATR programs at Raytheon. Abhijit received his BS degree with honors from the University of California, Santa Barbara, in 1984 and joined the Carnegie Mellon University, where received his MS and PhD degrees in 1985 and 1987, respectively. Prior to joining Raytheon, Abhijit was with Martin Marietta, Orlando, and was a faculty member at the University of Arizona. Abhijit is an associate editor for the journal of the Pattern Recognition Society, he is frequent reviewer of papers for optics journals, and he serves on the organizing committee for the SPIE conference in Orlando. Abhijit received the Hughes Business Unit Patent Award in 1998, and was elected fellow of SPIE in 1997 for his work on automatic target recognition.